Energy, exergy, economic and environmental assessment of the triangular solar collector assisted heat pump

Yan Jiang [a, c], Huan Zhang [a, c], Rui Zhao [a, c], Yaran Wang [a, c, *], Minzhang Liu [b, *],Shijun You [a, c], Zhangxiang Wu [a, c], Zhikai Liu [a, c], Shen Wei [d]

[a] School of Environmental Science and Engineering, Tianjin University, Haihe Education Area, Jinnan District, Tianjin 300350, PR China

[b] School of Energy and Safety Engineering, Tianjin Chengjian University, Tianjin 300384, PR China

[c] Tianjin Key Lab of Biomass/Wastes Utilization, Tianjin 300350, PR China

[d] The Bartlett School of Construction and Project Management, University College London (UCL), 1-19 Torrington Place, London WC1E 7HB, United Kingdom

Abstract

The solar air collector assisted air source heat pump is demonstrated to be an efficient clean heating technology, while the research on its working modes, and the corresponding energy, exergy, economic, environmental (4E) analysis is insufficient. In this study, a novel triangular solar air collector assisted air source heat pump (TSAHP) for building heating is proposed, and three working modes including preheating, series and parallel modes are illustrated. The energy model is established and used to determine the optimal working mode, and solved by Python environment. Four scenarios including TSAHP with three areas of triangular solar air collector (TSAC) and conventional air source heat pump (ASHP) are compared based on the optimal

[*] *Corresponding author. Tel.: +8602227892626; fax: +8602227892626.*

E-mail addresses: yaran_wang@tju.edu.cn

[*] *Corresponding author. Tel.: +8602227892626; fax: +8602227892626.*

E-mail addresses: liuminzhang@tju.edu.cn

working mode. Thermodynamic performance of the four scenarios under different working conditions is analyzed, and result indicate that the TSAHP with 3 m^2 TSAC can reduce the power consumption and exergy destruction of ASHP components by 321.9 kWh and 784.6 MJ respectively during the whole heating period. Economic evaluation shows that TSAHP has the shortest payback period with moderate TSAC area, and has economic advantages at low nominal interest rate and high electric power cost with large TSAC area. In addition, based on the whole life cycle, 1 m^2 of TSAC can reduce CO_2 emission by more than 4500 kg.

Keywords:

solar assisted heat pump; heat transfer model; thermodynamic performance; economic evaluation;

Nomenclature		air	circulating air of TSAC
A	surface area (m^2)	comp	compressor
C	heat capacity (W/K)	exc	evaporator and condenser
c_p	specific heat capacitance (J/(kg·K))	fan	fan of evaporator and condenser
D	hole aperture of perforated	gc	glass cover
	corrugated absorber (m)	ho	insulation housing of TSAC
d	thickness (m)	hole	hole of perforated corrugated
d_{in}	inner diameter (m)	in	inlet
d_{out}	outer diameter (m)	inv	inverter
Ex_{dest}	exergy destruction (W)	mot	motor
h_{conv}	convective heat transfer coefficient	out	outlet
	($W/m^2/K$)	ref	refrigerant
h_{in}	convective heat transfer coefficient	sol	solar
	of the inside surface ($W/m^2/K$)	t	total
h_{out}	convective heat transfer coefficient	thr	capillary throttle
	of the outside surface ($W/m^2/K$)	*Greek symbols*	
h_{rad}	radiative heat transfer coefficient	α	absorptivity (-)
	($W/m^2/K$)	β	inclination angle (°)
I	solar irradiance (W/m^2)	ε	emissivity (-)
i	refrigerant enthalpy (J/kg)	ε_r	exchange efficiency (-)
ie	the effective interest rate (%)	η_{comp}	total compressor efficiency (%)
if	inflation rate (%)	$\eta_{est.pre}$	exergy efficiency of preheating

L	length (m)		mode (%)
m	mass flow rate (kg/s)	$\eta_{est.ser\&par}$	exergy efficiency of series and
n	beneficial years		parallel mode (%)
P	pressure (Pa)	η_{tf}	total finned efficiency (%)
P_h	porosity factor of perforated	κ	polytropic exponent (-)
	corrugated absorber (-)	k	heat conductivity coefficient
Q_{conv}	convective heat transfer (W)		(W/m/K)
Q_h	heating load of rural residence (W)	ρ	density (kg/m^3)
Q_{rad}	radiant heat transfer (W)	υ	specific volume (m^3/kg)
Q_{sol}	absorbed solar irradiance (W)	τ	transmissivity (-)
Q_u	net heat gain of TSAC (W)	ψ	exergy factor (W/kg)
r	nominal intertest rate (%)	ω	fan speed (rpm)
s	entropy (J/mol/K)	*Abbreviations*	
T	temperature (℃)	SAHP	solar-assisted heat pump
U	overall heat transfer coefficient	ASAHP	solar air collector assisted heat
	(W/m^2/K)		pump
v	specific volume (m^3/kg)	ASHP	air source heat pump
W	power (W)	TSAC	triangular solar air collector
y	heat transfer area percentage (%)	TSAHP	triangular solar air collector
Subscripts			assisted air source heat pump
ab	perforated corrugated absorber		

1. Introduction

Climate change has become an indisputable fact, and the earth has warmed by 1.47 ℃ due to human activities since the first industrial revolution (Sakellariou et al., 2021). Continuous temperature rise will cause irreversible damage to the earth's ecology, as reducing carbon emissions has become the consensus of human (Pater., 2019). China aims to have carbon dioxide emissions peak before 2030 and achieve carbon neutrality before 2060. According to data released by the International Energy Agency (IEA), China accounted for 25% of global carbon emissions in 2018, about 10 billion tons, and building heating emissions contribute about 550 million tons (Chen et al., 2022). Therefore, the development of clean heating technology has an important significance to achieve carbon peak and neutrality (Esen, 2000).

The solar-assisted heat pump technology (SAHP) has been introduced and researched, and is considered to be one of the most promising clean heating technologies in the near future (Song et al., 2021a). Long et al. (2019) proposed a SAHP system with a dual heat source integrated heat pump evaporator, which uses solar hot water coils to preheat the air entering the evaporator, thus improving the evaporation temperature and COP of the air source heat pump (ASHP). The COP of SAHP is increased by 15% as the temperature of the solar hot water coil rise from 14.6 ℃ to 39.5 ℃. Song et al. (2021b) compared a novel SAHP system with the traditional ASHP, and the SAHP system can make full use of solar and air energy. When the solar irradiance is 1000 W/m^2, the COP of the SAHP system is 0.39 higher than the traditional ASHP. Chen et al. (2020) tested SAHP performance in cold areas and achieved a COP of 4.92 on sunny days. During the whole heating season, the operating costs of SAHP are 65.6% lower than traditional ASHP. Liu et al. (2020) investigated SAHP system for low-energy residential buildings in Alpine regions, and compared with traditional ASHP, the SAHP system reduced energy consumption by 55.38% and increased COP by 109.43%.

The above literature review shows that the SAHP system is technically feasible, has higher COP than traditional ASHP, and is suitable for cold areas (Long et al., 2020; Afshari., 2017). But its thermodynamic performance (Esen et al., 2007; Afshari., 2019), economic feasibility and effect of carbon-emission reduction are a concern to the decision-makers, 4E (energy, exergy, economic and environmental) analysis addresses these issues (Rout et al., 2021). Singh et al. (2020a, 2020b) developed a batch-type

SAHP dryer, and experimented in both simple heat pump and the novel SAHP for drying bananas. It can be concluded that the SAHP performs better in all aspects, although the initial investment is higher than the simple heat pump, the total running cost is lower, and the payback period is 3.9 years. Treichel and A.Cruickshank (2021a; 2021b) economically analyzed the applicability of traditional heat pump and SAHP based on environmental parameters across Canada and the United States. The results showed that the SAHP is economically feasible in locations with high electricity rate or long heating periods. Cai et al. (2017) proposed a dual source multi-functional SAHP system and calculated the exergy loss of the system under different working modes. The components of maximum exergy loss vary under different working modes, and the performance optimization of each working modes should focus on these key components. Saloux et al. (2019) compared and evaluated the exergo-economy of the SAHP system and the ASHP used for building heating. Two-dimensional exergy diagram was used to illustrate the dynamic exergy performance of both systems, and the SAHP is considered to have the best exergy efficiency. Ural et al. (2021a; 2021b) tested the ASHP with fabric solar air collector, and evaluated its thermodynamic performance and economy. The results showed that the electrical consumption of the novel SAHP system decreased by 8%, total exergy efficiency values increased by 3.1% and the levelized cost of heating dropped by 11.8%.

Compared with the other SAHP system, solar air collector assisted heat pump (ASAHP) has advantages of simple structure, small initial investment, suitable for evaporator of ASHP, and air as a heat transfer fluid does not need anti-freezing and is

not afraid of leakage. Kegel et al. (2012) compared the annual energy consumption and utility cost of SAHP with solar water collector and ASAHP based on three different single detached residential houses in Canada, and the ASAHP demonstrated better energy savings and lower capital costs in all housing types. Treichel and A.Cruickshank (2021c) deemed that the water type solar collector is intrusive to the evaporator of ASHP, and ASAHP can reduce the secondary space cooling benefit and improve heating efficiency by preheating the inlet air. The above literatures illustrated that the ASAHP is an efficient and ideal residential heating method. However, to the authors' knowledge, the working mode of the ASAHP considered in the literatures is only limited to using the solar air collector to preheat the inlet air of the evaporator, while researches on the operation strategy of ASAHP are rare as the ASAHP is suitable for different working modes under variable operating conditions. Similarly, 4E analysis related to operation strategy of ASAHP under different working modes has not been researched till yet.

Considering the above gaps in the literature, the current work focuses on completing the working modes of the ASAHP to ensure that the ASAHP has a corresponding most efficient working mode under different operating conditions, and the ASAHP is 4E analyzed under the optimal operation strategy to comprehensively illustrate the feasibility of the system. A novel triangular solar air collector (TSAC) is used as components of the ASAHP (TSAHP), and can penetrate more solar irradiance with tilted glass cover. The contents of this research are as the following: (1) COP was used as a standard to determine the optimal working mode under different operating

conditions based on the energy model; (2) Exergy performance of ASAHP systems on four scenarios were compared and analyzed. (3) Economic methods consist of *ATC*, *LCC* and *PP* were used to evaluate the economic viability of the ASAHP. (4) ASAHP carbon emissions based on the whole life cycle were calculated and compared.

2. System description

This chapter describes the working modes and mathematical model of TSAHP, and the schematic of the TSAHP system is shown in Fig. 1. The system consists of the TSAC, evaporator, condenser, rotary compressor, capillary throttle, fan, air duct and air valves (AV). The TSAC with tilted glass cover increases the heat collection area, and the perforated corrugated absorber (PCA) coated with chromium atomic deposition can efficiently absorb solar irradiance and transfer heat to the circulated air which is drawn into the TSAC through the upper air duct and discharged through the lower air duct (Jiang et al., 2021). The TSAHP system has three working modes under different operating conditions to achieve full utilization of solar energy. When solar irradiance and ambient temperature are low, AV 2 and 3 are opened, and the TSAHP in preheating mode. The outdoor air is heated by TSAC and enters the evaporator to improve evaporation temperature and heat pump efficiency. This working mode is designed to avoid low heat gain of indoor air into TSAC, as high temperature of indoor air causes large heat loss of TSAC. When solar irradiance and ambient temperature are high, AV 1 and 4 are opened, and the TSAHP in series mode. The indoor air is heated by TSAC and condenser successively, and returned to the room. This working mode is designed to avoid a drop in thermal comfort due to insufficient circulating air outlet temperature

(the threshold for this research is 25℃). When the outlet temperature of the circulating air exceeds 25 ℃, AV 1 and 5 are opened, and the TSAHP in parallel mode, and the circulating air returns directly to the room. The geometric and physical parameters of TSAHP system are shown in Appendix. A.

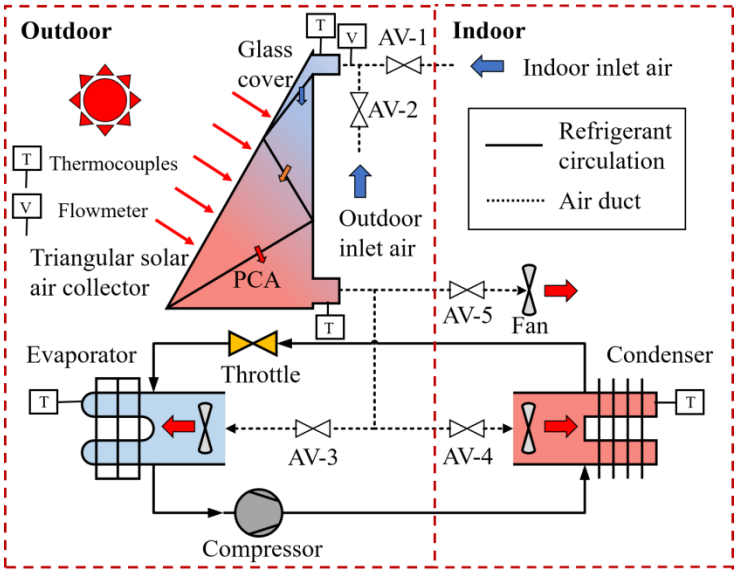

Fig. 1. Schematic of the TSAHP system.

3. Method

3.1. Assumptions

The mathematical model is developed to evaluate the 4E of TSAHP system, and some assumptions are considered for simplicity:

a) There is no heat loss in air ducts and refrigerant circulation pipes.

b) The pressure drop in the air ducts and refrigerant circulation pipes are ignored.

c) The TSAHP system is operating in steady state.

d) The circulating air and refrigerant are one–dimensional steady flows.

e) The thermal properties of the system are temperature-independent except for circulating air and refrigerant.

3.2. Energy model

TSAC is divided into glass cover, PCA, circulating air and insulation housing. The heat transfer relationship consists of convection and radiation heat transfer between the four parts of TSAC and outdoor environment. The radiation heat transfer inside TSAC is solved based on Kirchhoff's irradiance law, and other heat transfer terms are calculated by empirical formulas, as shown in Appendix. B. The energy conservation equations are as follows:

$$Q_{\text{sol.gc}} + Q_{\text{conv.gc-outdoor}} + Q_{\text{conv.gc-air}} + Q_{\text{rad.gc-outdoor}} + Q_{\text{rad.gc-ab}} + Q_{\text{rad.gc-ho}} = 0 \quad (1)$$

$$Q_{\text{sol.ab}} + Q_{\text{conv.ab-air}} + Q_{\text{conv.hole}} + Q_{\text{rad.ab-gc}} + Q_{\text{rad.ab-ho}} + Q_{\text{rad.ab-ab}} = 0 \quad (2)$$

$$Q_{\text{conv.ho-air}} + Q_{\text{conv.hole}} + Q_{\text{conv.gc-air}} + Q_{\text{conv.ab-air}} + Q_{\text{u.air}} = 0 \quad (3)$$

$$Q_{\text{conv.ho-air}} + Q_{\text{rad.ho-gc}} + Q_{\text{rad.ho-ab}} + Q_{\text{rad.ho-ho}} = 0 \quad (4)$$

Evaporator and condenser are finned-tube heat exchangers. The energy conservation equation and heat transfer equation between refrigerant and air based on heat transfer unit (NTU) method are as follows:

$$Q_{\text{conv.exc-air}} = m_{\text{ref}} \left(i_{\text{out}} - i_{\text{in}} \right) \quad (5)$$

$$Q_{\text{conv.exc-air}} = \varepsilon_{r.\text{exc-air}} C_{\text{air}} (T_{\text{air}} - T_{\text{ref}}) \quad (6)$$

The heat exchange efficiency $\varepsilon_{\text{r.exc-air}}$ and air thermal capacitance rate of refrigerant in single-phase and two-phase regions are calculated by empirical formulas, as shown in Appendix. C.

The compression process is considered as isentropic compression, and the polytropic model is used to describe the refrigerant compression process (Armstrong et al., 2014).

$$\frac{P_{\text{comp.out}}}{P_{\text{comp.in}}}=\left(\frac{v_{\text{comp.in}}}{v_{\text{comp.out}}}\right)^{\kappa} \tag{7}$$

$$\kappa=\frac{\ln\left(P_{\text{comp.out}}/P_{\text{comp.in}}\right)}{\ln\left(\rho_{\kappa}/\rho_{\text{comp.in}}\right)} \tag{8}$$

The total input power of compressor consists of motor power and inverter loss, the motor power of compressor is calculated by introducing the combined efficiency, and the inverter loss is considered as a linear function of motor power (Safijahanshahi et al., 2019).

$$W_{\text{comp}}=W_{\text{mot}}+W_{\text{inv}} \tag{9}$$

$$W_{\text{mot}}\times\eta_{\text{comb}}=m_{\text{ref}}\left(\frac{\kappa}{\kappa-1}\right)\left(\frac{P_{\text{comp.in}}}{\rho_{\text{comp.in}}}\right)\left(\left(\frac{P_{\text{comp.out}}}{P_{\text{comp.in}}}\right)^{\frac{\kappa-1}{\kappa}}-1\right) \tag{10}$$

$$\eta_{\text{comb}}=-0.145+1.213\exp\left(-0.04\frac{P_{\text{comp.out}}}{P_{\text{comp.in}}}\right) \tag{11}$$

$$W_{\text{inv}}=0.0153W_{\text{mot}}+23.4 \tag{12}$$

The refrigerant is isenthalpic at the inlet and outlet of the capillary throttle.

$$i_{\text{thr.out}}=i_{\text{thr.in}} \tag{13}$$

Evaporator and condenser fans are also considered. The input power of the fan depending on the angular velocity is calculated as follows (Zakula et al., 2011).

$$W_{\text{fan}}=1.48\times10^{-7}\omega^{2.832} \tag{14}$$

$$\omega=1602.6m_{\text{air}}v_{\text{air}}+57.8 \tag{15}$$

The COP is a key parameter to evaluate the energy efficiency of TSAHP under three working modes, which can be calculated as:

$$\text{COP}=Q_{\text{h}}/\left(W_{\text{comp}}+W_{\text{fan}}\right) \tag{16}$$

The energy model of TSAHP system has been verified in literatures (Jiang et al., 2021; Jiang et al., 2022). The absolute error of evaporation temperature is less than 2 ℃, the average relative error of COP is 7%. The average and maximum relative errors of the net heat gain are 4.6% and 10.8%, respectively. During the test, the average uncertainty of the recirculation air net heat gain was 12.3%. By comparing the above data, the model is reliable.

3.3. Exergy analysis

The exergy models of the TSAHP system components are elaborated based on the second law of thermodynamics. The exergy balance equation of the TSAC consists of input exergy of the solar irradiance, input and output exergy of the circulating air and exergy destruction (Hassan et al., 2021).

$$Ex_{\text{dest.TSAC}} = \psi_{\text{sol}} Q_{\text{sol}} - m_{\text{air}} (\psi_{\text{air.out}} - \psi_{\text{air.in}}) \tag{17}$$

The sun is assumed as infinite thermal source and temperature is equivalent to 6000 K. The exergy factor of solar irradiance is written as (Petela et al., 2003):

$$\psi_{\text{sol}} = 1 - \frac{4}{3}\left(\frac{T_{\text{outdoor}}}{T_{\text{sol}}}\right) + \frac{1}{3}\left(\frac{T_{\text{outdoor}}}{T_{\text{sol}}}\right)^4 \tag{18}$$

The solar irradiance absorbed by TSAC is calculated as the following:

$$Q_{\text{sol}} = Q_{\text{sol.gc}} + Q_{\text{sol.ab}} \tag{19}$$

The exergy of air at state (i) with environment as the reference state can be calculated as follows:

$$\psi_{\text{air.i}} = i_{\text{air.i}} - i_{\text{air.outdoor}} - T_{\text{outdoor}} \left(s_{\text{air.i}} - s_{\text{air.outdoor}}\right) \tag{20}$$

The exergy balance equation of the evaporator and condenser consists of input and output exergy of refrigerant and air, and exergy destruction. The exergy of refrigerant in state (i) also takes environment as the reference state.

$$Ex_{\text{dest.exc}} = m_{\text{air}}(\psi_{\text{air.in}} - \psi_{\text{air.out}}) + m_{\text{ref}}(\psi_{\text{ref.in}} - \psi_{\text{ref.out}}) \tag{21}$$

$$\psi_{\text{ref.i}} = i_{\text{ref.i}} - i_{\text{ref.outdoor}} - T_{\text{outdoor}}\left(s_{\text{ref.i}} - s_{\text{ref.outdoor}}\right) \tag{22}$$

The exergy balance equation of the rotary compressor and capillary throttle can be expressed as follows.

$$Ex_{\text{dest.comp}} = W_{\text{comp}} - m_{\text{ref}}(\psi_{\text{ref.out}} - \psi_{\text{ref.in}}) \tag{23}$$

$$Ex_{\text{dest.thr}} = m_{\text{ref}}(\psi_{\text{ref.in}} - \psi_{\text{ref.out}}) \tag{24}$$

The exergy efficiency is the ratio of effective exergy and input exergy. When the TSAHP system is on preheating mode, the condenser provides indoor heating, and the exergy efficiency of TSAHP system is written as:

$$\eta_{\text{est.pre}} = \frac{m_{\text{air}}\left(\psi_{\text{con.air.out}} - \psi_{\text{con.air.in}}\right)}{\psi_{\text{sol}}Q_{\text{sol}} + W_{\text{comp}} + W_{\text{fan}}} \tag{25}$$

When the TSAHP system is on series and parallel modes, the TSAC and condenser provide indoor heating, and the exergy efficiency of TSAHP system can be calculated as:

$$\eta_{\text{est.ser\&par}} = \frac{m_{\text{TSAC.air}}\left(\psi_{\text{TSAC.air.out}} - \psi_{\text{TSAC.air.in}}\right) + m_{\text{con.air}}\left(\psi_{\text{con.air.out}} - \psi_{\text{con.air.in}}\right)}{\psi_{\text{sol}}Q_{\text{sol}} + W_{\text{comp}} + W_{\text{fan}}} \tag{26}$$

3.4. Economic method

One of the evaluation methods of economic process is annual total cost (*ATC*), which consists of the annual maintenance cost (*AMC*), annual electric power cost (*AEPC*), and annual cost of initial cost (*IC*) and system salvage value (*SV*). *AEPC* is

the product of the electric power cost and the power consumption of the compressor and fan during the heating season. The other economic parameters of TSAHP system are presented in Table. 1 (Jiang et al., 2021).

$$ATC = AMC + AEPC + IC\left(\frac{ie(1+ie)^n}{(1+ie)^n - 1}\right) - SV\left(\frac{ie}{(1+ie)^n - 1}\right) \tag{27}$$

The effective interest rate (*ie*) can be calculated by the nominal interest rate (r) and the inflation rate (*if*).

$$ie = (1+r)/(1+if) - 1 \tag{28}$$

The life cycle cost (*LCC*) method can represent tomorrow's cost with today's prices (Kavian et al., 2020), and the *LCC* method considers the *IC* and present value of *AMC*, *AEPC* and *SV*.

$$LCC = IC + (AMC + AEPC)\frac{(1+ie)^n - 1}{i(1+ie)^n} - SV\frac{1}{(1+ie)^n} \tag{29}$$

In addition, to better evaluate the economic performance of the TSAHP system, the levelized cost of heating (*LCOH*) as the ratio of LCC and the present value of annual heating capacity (*AHC*) is proposed as follows:

$$LCOH = LCC/\left(AHC\frac{(1+ie)^n - 1}{ie(1+ie)^n}\right) \tag{30}$$

Compared to the traditional ASHP, the TSAHP coupled with the TSAC leads to the growth in *IC*, while saving electricity and thus reducing the *ATC*. The payback period (*PP*) for the TSAHP is defined as follows:

$$PP = \frac{IC_{\text{TSAHP}} - IC_{\text{ASHP}}}{ATC_{\text{ASHP}} - ATC_{\text{TSAHP}}} \tag{31}$$

Table. 1. The economic parameters of TSAHP system (Jiang et al., 2021).

Parameter	Value
IC of ASHP	500 $
IC of TSAC	54 $/m^2
AMC	10% of *ATC*
SV	5% of *IC*
Electric power cost	0.14 $/(kWh)
n	20 years
r	1.75%
if	3.41%

3.5. Environmental impacts

Compared with the conventional ASHP, the TSAHP with TSAC can reduce the annual electric power consumption (*AEP*) and CO_2 emission during system operation. However, it is inappropriate to merely consider the CO_2 emission reduction during the operation, as the TSAC cause energy consumption and CO_2 emission in the production, transportation and dismantling process. Therefore, the CO_2 emission reduction performance of the TSAHP based on the whole life cycle is analyzed. Considering the loss of power transmission and distribution, the generation of 1 kWh electricity emit 2 kg of CO_2 (Deniz et al., 2016), and the CO_2 emission reduction of the TSAHP during operation ($ERCO_{2op}$) is calculated as follows:

$$ERCO_{2op} = (AEP_{ASHP} - AEP_{TSAHP}) \times n \times 2 \tag{32}$$

The CO_2 emission in the production process of TSAC (ECO_{2pro}) is the product of the materials consumption (*MC*) and the CO_2 emission factors ($C_{ef}1$), the dismantling process (ECO_{2dis}) is 10% of the production process, and the transportation (ECO_{2tra}) process should be considered in the transportation distance (*TD*) and carbon emission factor per unit distance ($C_{ef}2$). The CO_2 emission parameters during TSAC production and transportation are shown in Table. 2. The CO_2 emission of each process and the

CO_2 emission reduction performance of the TSAHP based on the whole life cycle ($ERCO_{2wlc}$) can be calculated by the following equations:

$$ECO_{2pro} = \sum(MC \times C_{ef}1) \tag{33}$$

$$ECO_{2tra} = \sum(MC \times TD \times C_{ef}2) \tag{34}$$

$$ERCO_{2wlc} = ERCO_{2ope} - ECO_{2pro} - ECO_{2dis} - ECO_{2tra} \tag{35}$$

Table. 2. The CO_2 emission parameters of TSAC.

	MC of 1m^2 TSAC	Cef1	TD	Cef2
Glass cover	11.5 kg Polycarbonate	1.1 kg CO_2/kg	500 km	0.3 kg CO_2/(t·km)
PCA	1.7 kg Stainless steel	2.3 kg CO_2/kg	500 km	0.3 kg CO_2/(t·km)
Insulation	4.8 kg Polystyrene board	5.0 kg CO_2/kg	500 km	0.3 kg CO_2/(t·km)
housing	6.3 kg galvanized sheet	2.8 kg CO_2/kg	500 km	0.3 kg CO_2/(t·km)

3.6. Numerical method

At the beginning of the 4E analysis, the energy model of TSAHP is solved to seek for the optimal working mode. The geometric parameters of TSAC, evaporator and condenser, and the physical parameters of corresponding materials are input. Boundary conditions are determined including heating load, indoor temperature, outdoor temperature and solar irradiation. The inlet temperature of the TSAC circulating air is outdoor temperature on preheating mode, or indoor temperature on series and parallel mode. The outlet temperature and net heat gain of circulating air are obtained by solving the TSAC energy model, and as the boundary conditions of the ASHP energy model according to the corresponding working modes. The COP of the three working modes is calculated and the working mode with the maximum COP is selected. Based on the optimal working mode, exergy loss of each component, different economic methods and CO_2 emission reduction during whole life cycle are calculated. The numerical

method is realized by Python environment, and the physical parameters of circulating air and refrigerant are calculated by the REFPROP package. The flowchart of the numerical method is shown in Fig. 2.

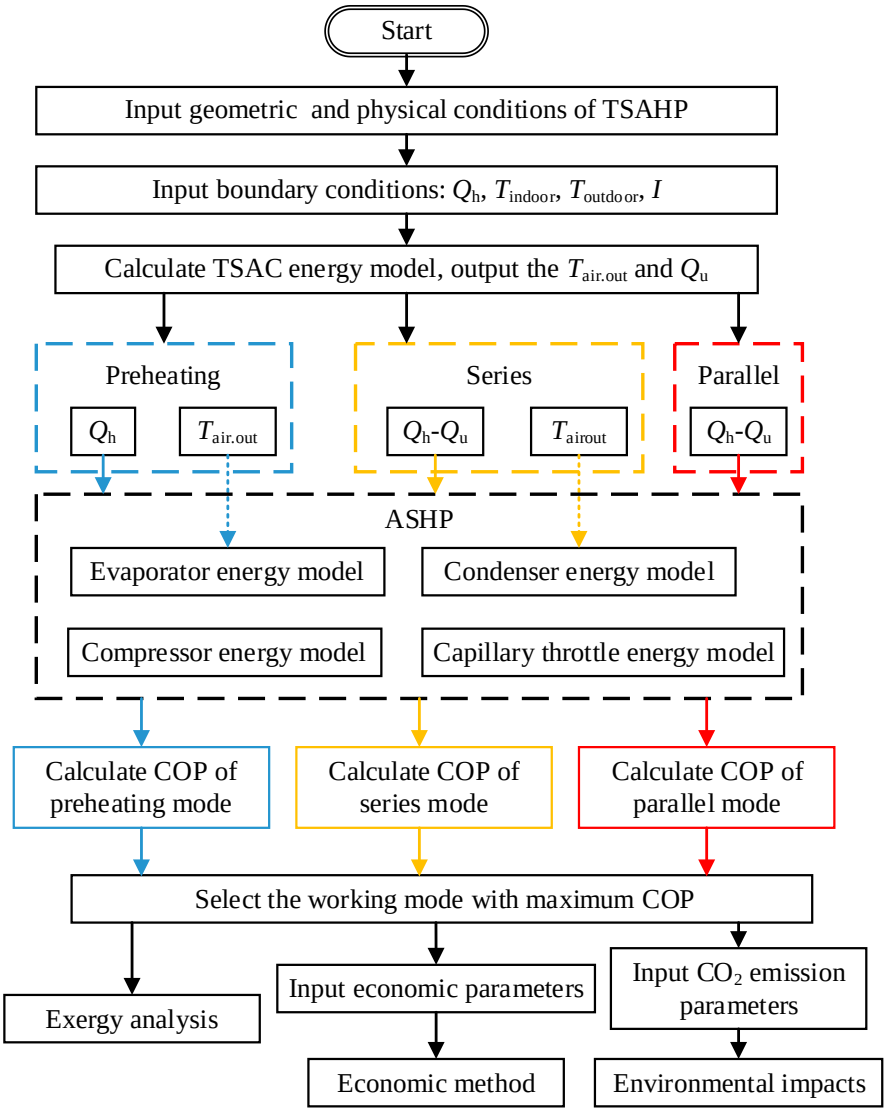

Fig. 2. Flowchart of the numerical method.

4. Result and discussion

To analyze the 4E performance of the TSAHP system, four scenarios including the TSAHP system with three different TSAC areas and the conventional ASHP are compared, as shown in Table. 3.

Table. 3. The describe of four scenarios.

Scenarios	Configuration
1	TSAHP system with 1 m^2 TSAC
2	TSAHP system with 2 m^2 TSAC
3	TSAHP system with 3 m^2 TSAC
4	Conventional ASHP

The key parameters that affect the exergy performance of TSAHP system are solar irradiance, outdoor temperature, indoor temperature and heating load of building. To investigate the effects of single parameter, the alternative parameters were set at standard values: I_{gc} = 600 W/m^2, $T_{outdoor}$ = 0 ℃, T_{indoor} = 18 ℃, Q_h = 2 kW.

4.1. Energy analysis

As shown in Fig.3, in the three TSAHP scenarios, with the growth of solar irradiance, energy consumption goes down and COP goes up as the circulating air outlet temperature of the TSAC is improved. On the preheating mode, the heated circulating air is directly blown into the evaporator, the evaporation temperature raises, and the compressor compression ratio and energy consumption fall down. On series and parallel modes, the net heat gain of the TSAC reduces the heat transfer demand by the condenser, thus reducing the compression ratio and energy consumption. The energy consumption of scenario 3 is the lowest, as TSAHP with larger TSAC area can use more solar energy. When the solar irradiance is 300 W/m^2, the working modes of the three TSAHP scenarios are changed from preheating mode to series mode, and the slope of energy consumption and COP rises. This is because the net heat gain of the TSAC is directly input into the room on series mode, while the net heat gain is input into the evaporator on preheating mode, which heat pump circulation is requires to enter the room. The scenario 2 and 3 is turned into parallel mode when the solar irradiance is 600

and 450W/m^2 respectively, while scenario 1 remained in series mode as the TSAC area is small and the outlet temperature of circulating air cannot reach the threshold. Compared with the series mode, the TSAC flow rate and heat loss of the parallel mode are minor, and the condensation temperature is not gone up as that under the series mode, therefore, the slope of energy consumption and COP is larger. As the heating load is constant, COP is inversely proportional to the energy consumption. Solar irradiance does not affect the energy consumption and COP of the scenario 4. When the solar irradiance is 900 W/m^2, COP of scenario 3 is 5.7 times that of scenario 4.

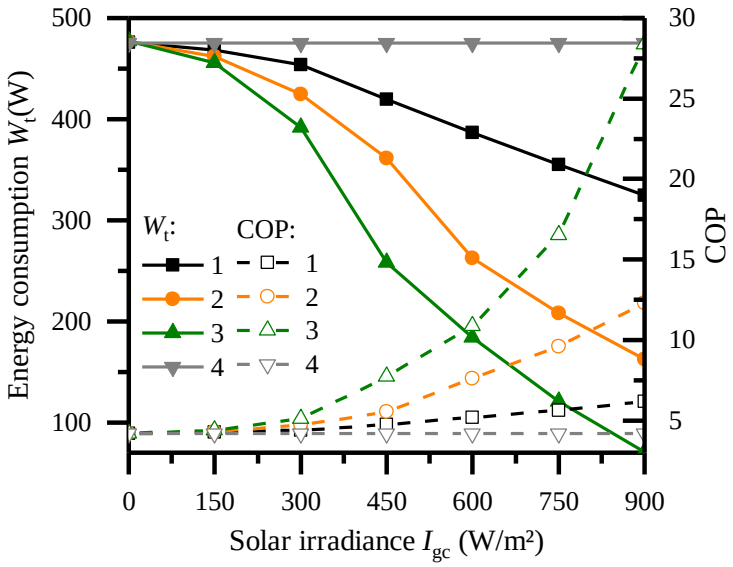

Fig. 3. The effect of solar irradiance on energy consumption and COP.

The effects of the outdoor temperature on the energy consumption and COP of the four scenarios are illustrated in Fig. 4. With the rise of outdoor temperature, the energy consumption of the TSAHP goes down, and COP increases, as the evaporation temperature raises. When the outdoor temperature is 0 ℃, the working mode of the scenario 2 changed from series mode to parallel mode, and energy consumption decreased significantly. With the enlargement of TSAC area, more net heat gain is

received and the energy consumption drops successively. When the outdoor temperature is -12 ℃, the difference of energy consumption between scenarios 1 and 2 is less than that between scenarios 2 and 3. This is because at -12 ℃, scenarios 1 and 2 are series mode but scenario 3 is parallel mode. When scenario 2 is transformed into parallel mode, the energy consumption is greatly reduced, and the difference of energy consumption between scenarios 1 and 2 is bigger than that between scenarios 2 and 3. With the rise of outdoor temperature, the energy consumptions of 4 scenarios decrease, and indoor heating load is constant, thus the COP raises and its slope increase. When the outdoor temperature rises from -12 to 12 ℃, COP difference between scenarios 3 and 4 ascends from 3.2 to 15.3.

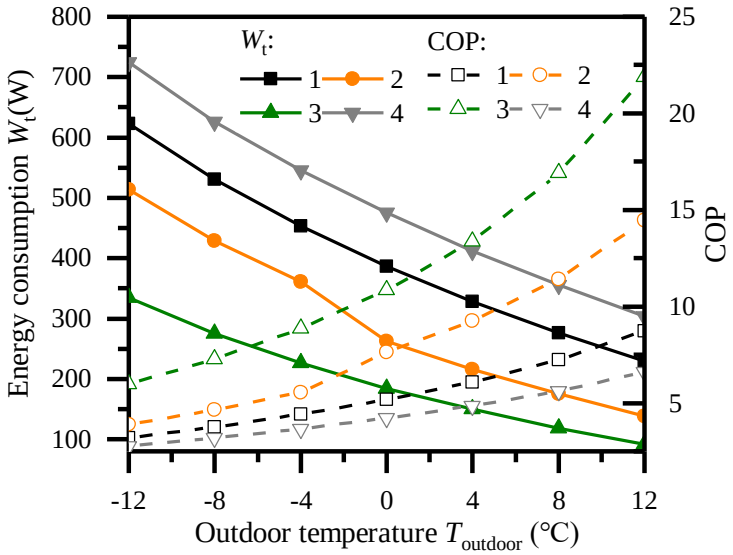

Fig. 4. The effect of outdoor temperature on energy consumption and COP.

Fig. 5 shows the effect of indoor temperature on the energy consumption and COP of the four scenarios. With the increase of indoor temperature, the condensation temperature and the compression ratio go up, thus the energy consumption goes up and the COP goes down. The scenario 2 and 3 are turned into parallel mode when the indoor

temperature is 18 and 16 ℃ respectively, as the energy consumption is dropped slightly and the COP has the same inflection point. At different indoor temperatures, the working modes of three TSAHP scenarios are series and parallel modes and the inlet temperature of the TSAC is the indoor temperature. When the indoor temperature is higher, the temperature difference between the TSAC and the outdoor increase, as the scenarios with large TSAC area has large heat loss and fast COP decrease. The COP difference between scenarios 3 and 4 is 7.5 when the outdoor temperature is 12 ℃, but only 4.4 when the outdoor temperature is 24 ℃.

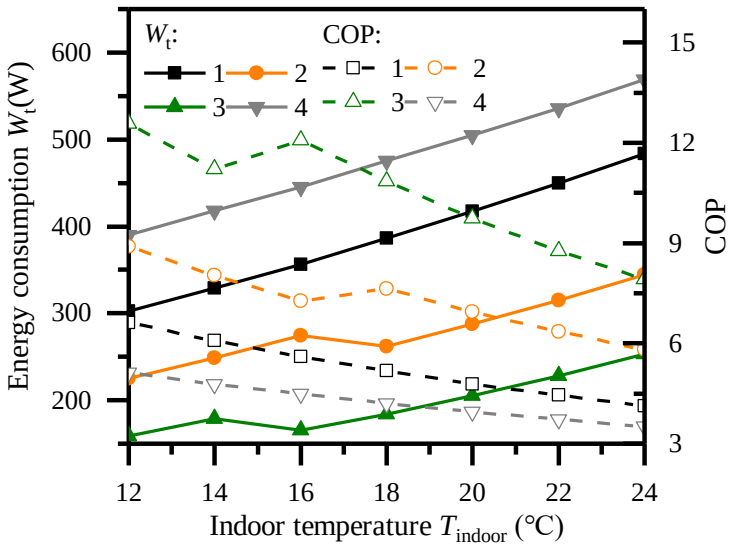

Fig. 5. The effect of indoor temperature on energy consumption and COP.

The effects of the heating load on the energy consumption and COP of the four scenarios are illustrated in Fig. 6. As the heating load increases, the compression ratio and the energy consumption of the compressor raises, in addition, the fan air volume and the fan power consumption of evaporator and condenser goes up, thus the system energy consumption increases. For scenario 3, when the heating load is 1000 kW, the TSAC can fully take on the heating load, and the heat pump does not work. When the

heating load rises, the excess load needs the heat pump to operate, as the working conditions and the net heat gain of TSAC are unchanged. The proportion of heating load operated by TSAC is reduced, and the effect of TSAC is weakened. Therefore, the COP of three TSAHP scenarios are gradually tends to the COP of scenario 4. However, when the heating load is 3000 W, the COP of scenario 3 is still 3.5 higher than that of scenario 4, indicating that TSAHP has obvious advantage under different heating loads.

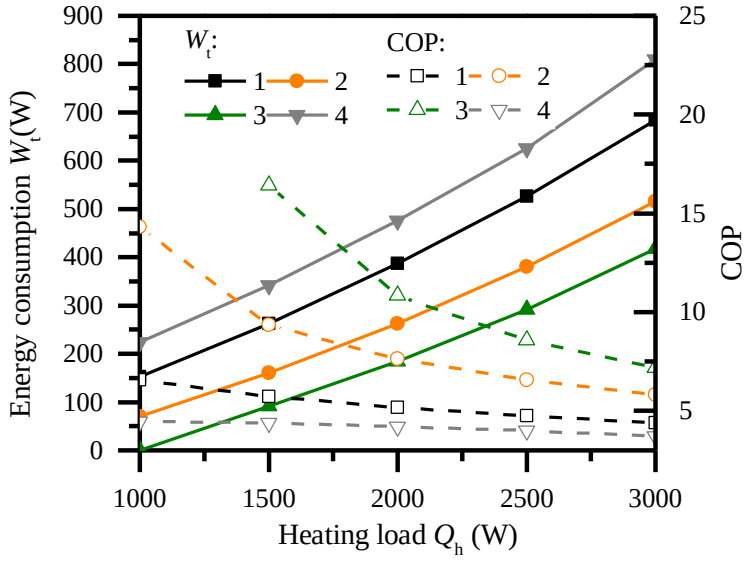

Fig. 6. The effect of heating load on energy consumption and COP.

To compare power consumption of the four scenarios under actual working conditions, a typical meteorological parameter in Tianjin, China (39.98 °N, 117.38 °E), and the heating load of a 36 m^2 rural residence under corresponding meteorological parameter was adopted for simulation. Geometric and physical parameters of the rural residence are listed in Appendix. A. Monthly power consumption of the four scenarios during the heating period are show in Fig. 7. Monthly power consumption is mainly affected by the outdoor temperature, and power consumption is the highest in January as the outdoor temperature is the lowest. The power consumption of scenario 3 in

January is 81.2 kWh greater than that in December, and that in scenario 4 is 104.6 kWh greater. In addition, the scenario with large TSAC area has low power consumption, and power consumption of scenario 4 is the largest in the whole heating period, which is 321.9 kWh larger than scenario 3.

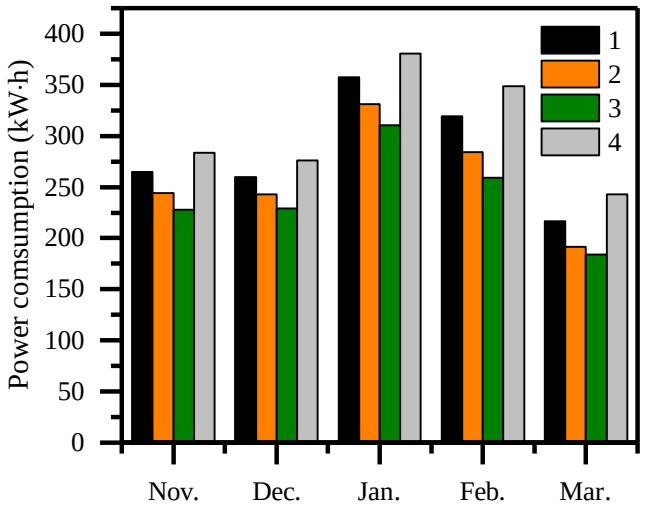

Fig. 7. The comparison of power consumption in heating period.

4.2. Exergy analysis

As shown in Fig.8, when the solar irradiance is below 150 W/m^2, the TSAHP system of the three scenarios are on the preheating mode, and the TSAC inlet temperature is outdoor temperature, as the TSAC has low circulating air temperature and little exergy destruction. With the rise of solar irradiance, the working modes of the three scenarios turn into series and parallel modes, and the TSAC inlet temperature is indoor temperature, the exergy destruction of TSAC and TSAHP increased. But the net heat gain of the TSAC falls off the heat transfer demand by the condenser, thus reducing the compression ratio and exergy destruction of TSAHP components other than TSAC, as the exergy destruction of TSAHP tends to be stable. The exergy destruction of TSAC

is the largest among the TSAHP components, and the maximum TSAC area of scenario 3 leads to the large exergy destruction. When the solar irradiance is 450 W/m^2, exergy destruction of the scenario 3 goes down significantly as working mode changed from series mode to parallel mode, and compared with the series mode, the TSAC flow rate and exergy destruction of the parallel mode are minor. With the rise of solar irradiance, effective exergy and input exergy increase simultaneously. On the preheating mode, the net heat gain of the TSAC is input into the evaporator, and the rise of effective exergy is slow and the exergy efficiency decreased, while on the series and parallel modes, the net heat gain of TSAC is directly used for space heating, thus the exergy efficiency gone up, and exergy efficiency of scenario with large TSAC area is higher. Solar irradiance does not affect the exergy destruction and exergy efficiency of the scenarios 4, and when the solar irradiance is higher than 300 W/m^2, the exergy efficiency of the TSAHP system is higher than that of the scenarios 4.

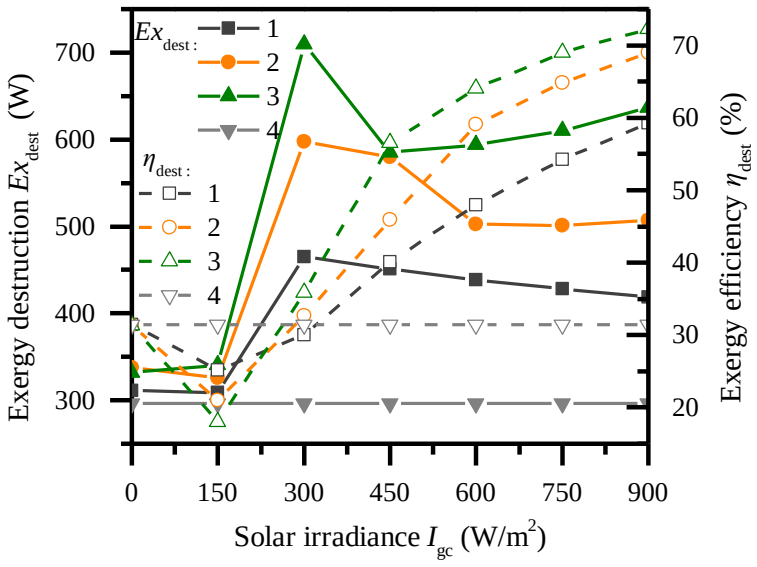

Fig. 8. The effect of solar irradiance on exergy destruction and exergy efficiency.

Fig. 9 shows the effect of outdoor temperature on the exergy destruction and exergy efficiency of four scenarios. With the growth of outdoor temperature, the exergy destruction of the ASHP decreases, as the evaporation temperature raises and the compressor compression ratio falls down. In addition, the exergy destruction of TSAC decreased, leading to a larger decrease of the TSAHP exergy destruction than that of conventional ASHP. When the outdoor temperature is 0 ℃, the working mode of the scenario 2 changed from series mode to parallel mode, and exergy destruction decreased significantly. With the growth of outdoor temperature, the effective exergy and input exergy of scenarios 4 drop, and the exergy efficiency raises first and then drops. While the effective exergy of TSAC increase leading to the exergy efficiency of TSAHP ascend and exergy efficiency of scenario with large TSAC area is higher. When the outdoor temperature rises from - 12 to 12 ℃, the difference of exergy efficiency between the scenarios 1 and 4 ascends from 23% to 50%, which indicated that the TSAHP is superior at higher outdoor temperatures.

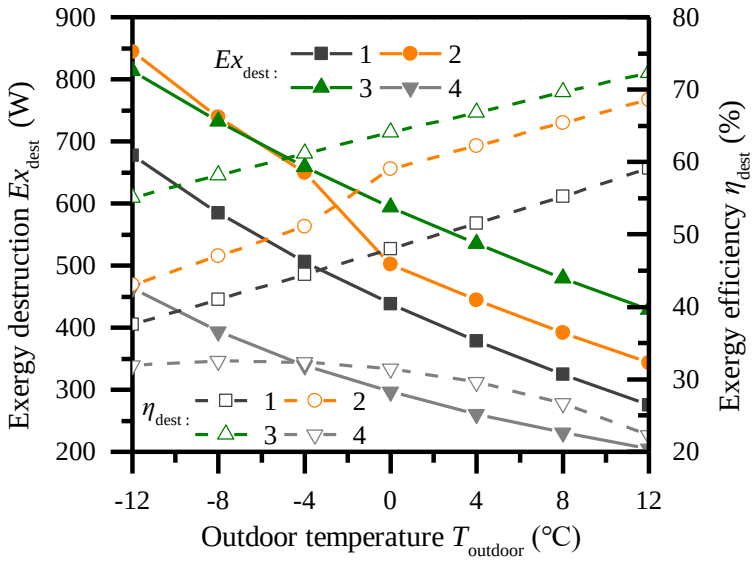

Fig. 9. The effect of outdoor temperature on exergy destruction and exergy efficiency.

The effects of the indoor temperature on the exergy destruction and exergy efficiency of four scenarios are illustrated in Fig. 10. With the increase of indoor temperature, the condensation temperature and the compression ratio go up, thus exergy destruction of ASHP ascend. At different indoor temperatures, the inlet temperature of the TSAC is the indoor temperature, thus the exergy destruction of the TSAC goes up with the raise of the indoor temperature. To the combined effect of the ASHP and TSAC, exergy destruction of TSAHP significantly enhance. On series and parallel modes, the effective exergy of TSAHP is provided by condenser and TSAC. The effective exergy of condenser increases as the outlet temperature of condenser raises, while the decline of TSAC effective exergy leads to the descend of overall effective exergy. Besides, input exergy also goes up as the condensation temperature and the compression ratio raised, and the exergy efficiency of TSAHP goes down. With the increase of condenser effective exergy and input exergy, the exergy efficiency of scenarios 4 increases slowly.

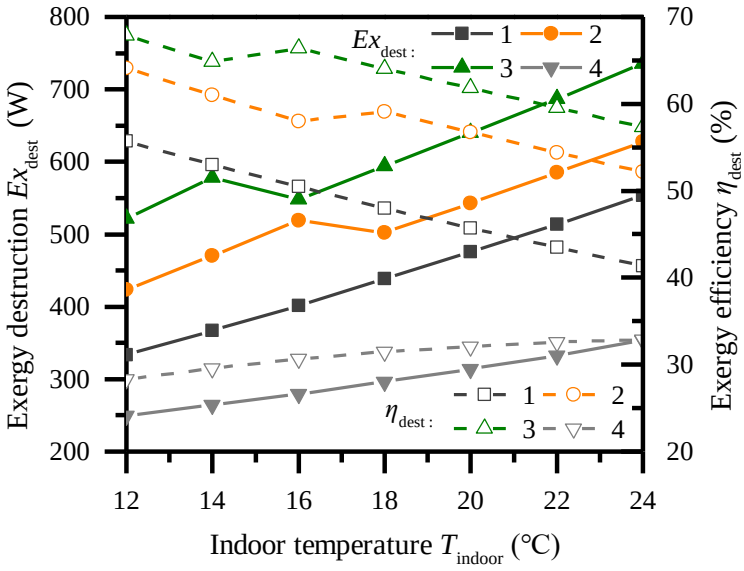

Fig. 10. The effect of indoor temperature on exergy destruction and exergy efficiency.

The effects of the heating load on the exergy destruction and exergy efficiency of four scenarios are illustrated in Fig. 11. With the ascend of the heating load, compression ratio goes up, thus the exergy destruction of ASHP and four scenarios are raised. As the heating load enhance, the air flow of evaporator and condenser increases. For scenario 1, the working mode under different heating loads is series mode, and the air flow of TSAC is equal to that of condenser, thus the exergy destruction of TSAC increases. While the TSAC exergy destruction of scenarios 2 and 3 remains as they operate on parallel mode with constant TSAC air flow. To the combined effect of the ASHP and TSAC, exergy destruction of scenario 1 rise larger than scenarios 2 and 3. With the heating load and compression ratio go up, the outlet temperature of the condenser and effective exergy raise, but the input exergy also goes up, and the exergy efficiency of four scenarios goes down slowly. The effective exergy of TSAHP is provided by both TSAC and condenser, thus the exergy efficiency of TSAHP is higher than that of scenarios 4, and exergy efficiency increases with the enhance of TSAC area.

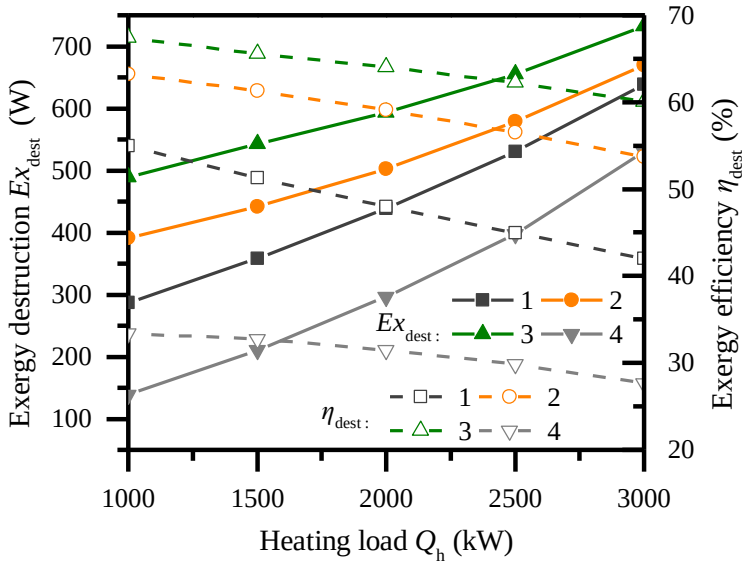

Fig. 11. The effect of heating load on exergy destruction and exergy efficiency.

Typical daily meteorological parameters on January 19 of Tianjin (39.98°N, 117.38°E) are shown in Fig.12 (a). As shown in Fig. 12 (b). the exergy efficiency and COP of scenario 4 change little on the combine effect of heating load and outdoor temperature, while the exergy efficiency and the COP of TSAHP are mainly affected by solar irradiation. From 8:00 to 9:00, the solar irradiation and outdoor temperature are small, and the working mode of TSAHP is preheating mode. The exergy efficiency is descended as the effective exergy growth slower than input exergy, which also appeared at 17:00 to 18:00. At other times, the change of exergy efficiency is consistent with solar irradiance, and the exergy efficiency of TSAHP with large TSAC area is higher. With the TSAC area increases, the growth rate of effective exergy and exergy efficiency go down. The average exergy efficiency of scenario 2 is 16.1% higher than that in scenario 1, while average exergy efficiency of scenario 4 is only 4.6% higher than that in scenario 3. From 8:00 to 18:00, the COP of the scenario with large TSAC area is higher, and the COP growth rate raises with the rise of TSAC area, as the reduction rate of compressor power consumption goes up. The average COP of scenario 1 to scenario 4 is 4.3, 5.8, 9.8, and 3.7, respectively. Safijahanshahi and Salmanzadeh proposed a SAHP system with transpired SAC, which could improve COP by 17.4% compared with the traditional ASHP under the operating condition close to 11:00. However, the COP of the TSAHP system in this study increase by 152% at 11:00, as the TSAHP system adopted the optimal working mode under different operating condition, instead of the single preheating mode in the literature.

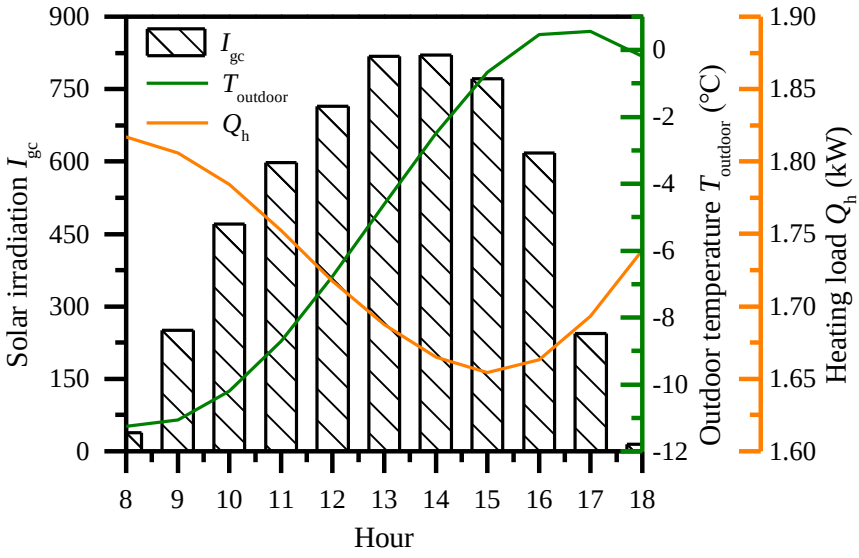

(a)

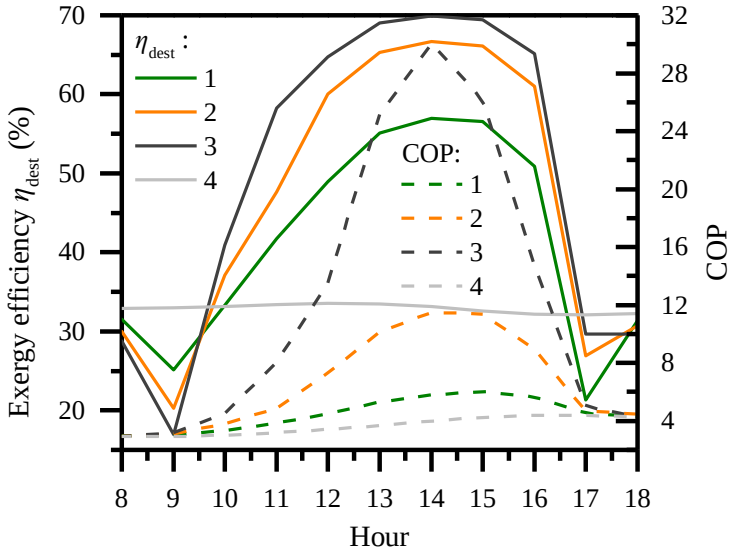

(b)

Fig. 12. The comparison on exergy efficiency and COP of four scenarios.

Monthly exergy destruction of four scenarios during the heating period are show in Fig. 13(a). Monthly exergy destruction is mainly affected by the outdoor temperature, and exergy destruction is the highest in January as the outdoor temperature is the lowest. In addition, the scenario with large TSAC area is greatly affected by outdoor temperature, as the exergy destruction of the TSAC raises rapidly with the decline of

outdoor temperature. The exergy destruction of scenario 3 in January is 393.2 MJ greater than that in December, while that in scenario 1 is only 313.8 MJ greater. Exergy destruction of scenario 3 is the largest in the whole heating period, which is 1637.3 MJ larger than scenario 4. Fig. 8(b) shows the components exergy destruction of four scenarios, and exergy destruction of TSAC and compressor is much greater than other components, accounting for 62.6% of the total exergy destruction in scenario 4 and 80.7% in scenario 1. With the area and exergy destruction of TSAC increase, exergy destruction of other components goes down. Exergy destruction of other components except the TSAC in scenario 1 and 3 decreased by 321.2 MJ and 784.6 MJ compared with scenario 4, as TSAC can effectively reduce the compression ratio of the compressor and the heat exchange temperature difference of the evaporator and condenser. In addition, the exergy destruction of the TSAC can be significantly reduced by using the double glass cover.

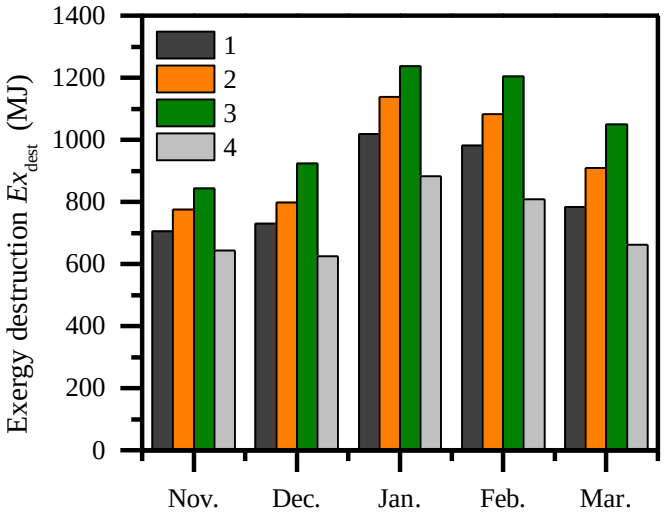

（a）

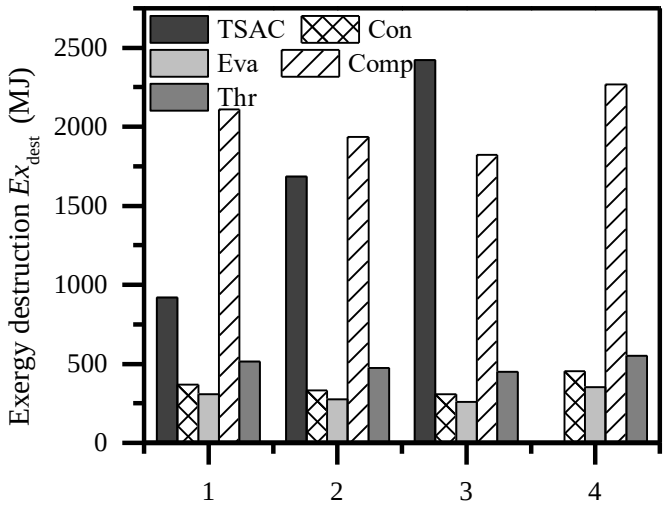

(b)

Fig. 13. The comparison of exergy destruction in heating period.

4.2. Economic analysis

The economic evaluation methods including *IC*, *ATC*, *LCC* and *LCOH* of four scenarios are comprehensively compared, as shown in Fig. 14. With the growth of TSAC area, the *IC* and *AMC* of TSAHP increase, while the *AEPC* goes down. Based on the 20 beneficial years of TSAHP, the *AEPC* is the main parameter that affects the economic evaluation method, as the *ATC*, *LCC* and *LCOH* of the TSAHP with large TSAC area are smaller. The *ATC* of scenario 3 is 12.1% lower than that of scenario 1, and the minimum and maximum *LCC* belong to scenario 3 and scenario 4 with values of 5311.3 and 6384.4, respectively. The *LCOH* of scenario 4 is 0.048 $/kWh and lower than the electric power cost of 0.14 $/kWh, as the average COP of ASHP is higher during the heating period. Similarly, heating performance of TSAHP is further improved, with *LCOH* reduced by 18.4 % of scenario 3 compared to scenario 4.

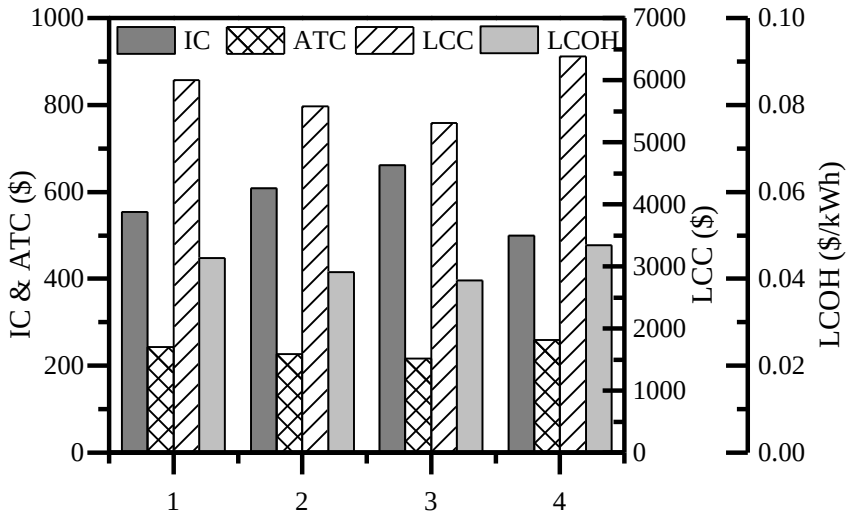

Fig. 14. The comparison of economic evaluation methods in heating period.

Fig. 15 shows the effects of nominal interest rate on the *LCC* and *PP* of four scenarios. With the ascend of nominal interest rate, present values of *AMC* and *AEPC* are decreased, thus the *LCC* of four scenarios are descend. The nominal interest rate has a greater impact on the scenarios with high *AEPC* as the present value of *AEPC* is significantly reduced. When the nominal interest rate increases from 0 to 10, the difference of *LCC* between scenario 3 and scenario 4 descends from 469.5 to 142.0. In addition, with the rise of nominal interest rate, the annual cost of *IC* and *ATC* ascends. As the *IC* of TSAHP is higher, the difference of *ATC* between TSAHP and conventional ASHP decreases, and the *PP* goes up. It is noticed that scenario 2 has the shortest *PP* as the *IC* of scenario 3 is higher and the AEPC and ATC of scenario 1 are higher, and the average *PP* of scenario 2 is 0.2 and 0.5 year shorter than the scenario 1 and scenario 3, respectively. This is indicated that the TSAHP has advantages at low nominal interest rate, and when the PP is the dominating economic parameter to be considered, a moderate TSAC area should be selected, which is 2 m^2 of scenario 2 in this research.

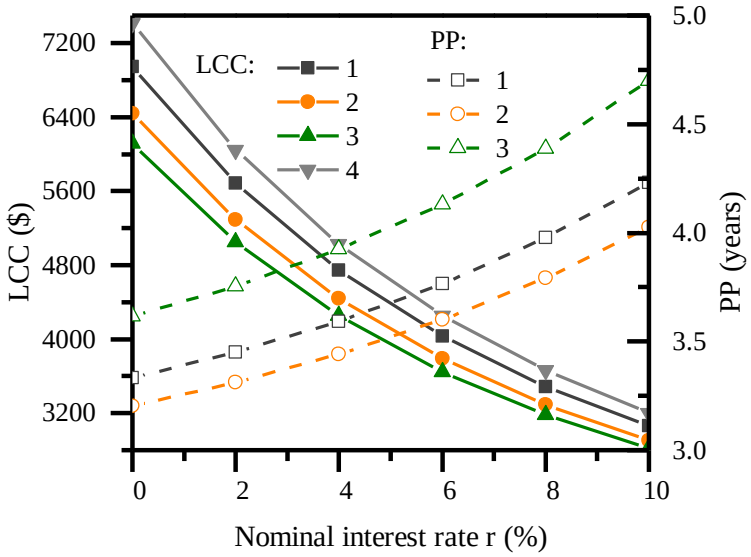

Fig. 15. The effect of nominal interest rate on the *LCC* and *PP*.

The effects of electric power cost on the *LCC* and *PP* of four scenarios are illustrated in Fig. 16. With the rise of electric power cost, the present value of *AEPC* and *LCC* go up, and the ascend of *LCC* is significant in the scenario of high *AEPC*. When the electricity power cost is 0.04, the *LCC* difference between the four scenarios is small, while when the electricity power cost is 0.2, the *LCC* of scenario 3 is 1546.7 higher than that of scenario 4. Besides, the TSAHP scenario saves a certain amount of electricity compared with scenario 4, while with the growth of electricity power cost, the saved *AEPC* and *ATC* increases and the *PP* is shortened. The scenario 3 is not desirable at an electric power cost of 0.04 as the *PP* is longer than 20 beneficial years. According to the above analysis, the TSAHP has advantages at high electric power cost, and when the electricity power cost is low, the TSAHP with larger TSAC area is not economically feasible.

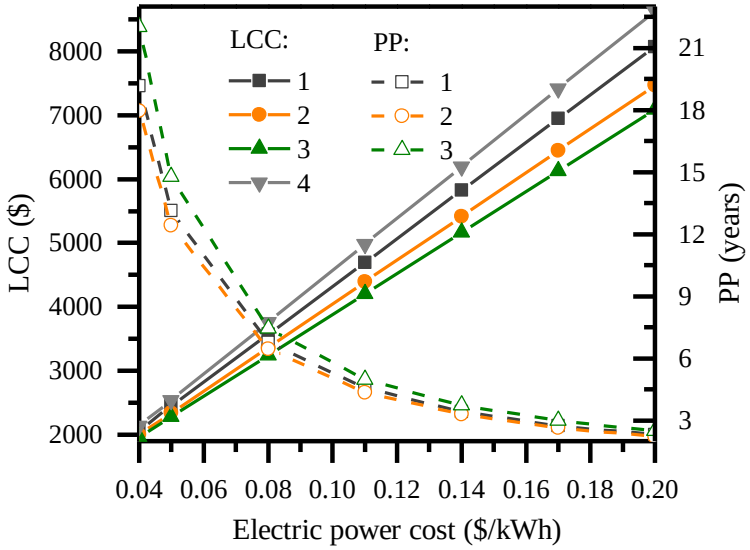

Fig. 16. The effect of electric power cost on the *LCC* and *PP*.

4.3. Environmental impacts analysis

Fig. 17 shows the CO_2 emission reduction performance of the TSAHP based on the whole life cycle. With the TSAC area increases, the consumption of *AEP* decreases, and the *AEP* of scenario 3 is 324 kWh/year less than that of scenario 4, which effectively reduces the CO_2 emission during operation of TSAHP system. However, CO_2 emissions during the production, dismantling and transportation of TSAC also ascend with the rise of TSAC area, and the scenario 3 is 135.3 kg more than that of scenario 1. The TSAC production leads to the largest CO_2 emissions, which are 16 times higher than the transportation. Considering the CO_2 emission of each TSAC process, the CO_2 emission reduction of scenario 1, scenario 2 and scenario 3 based on the whole life cycle is 4646.7, 9631.3 and 12960.8 kg, respectively. In other word. 1 m^2 of TSAC can reduce CO_2 emission by more than 4500 kg.

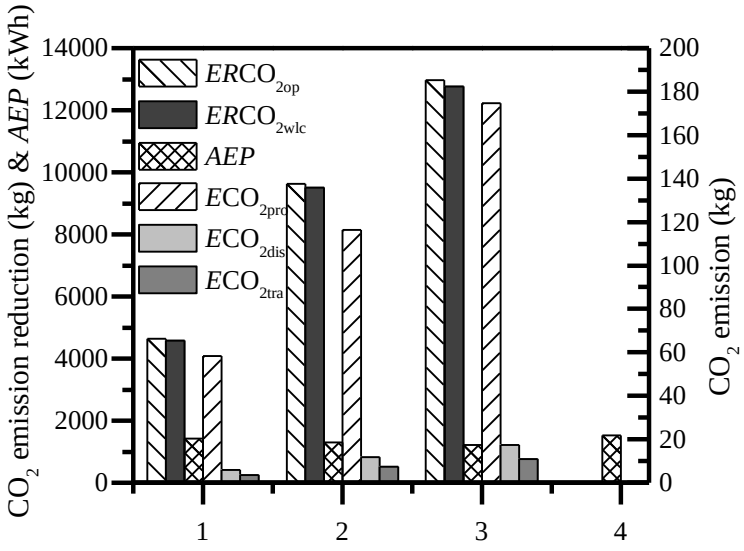

Fig. 17. The CO_2 emission reduction performance of the TSAHP scenarios.

5. Conclusions

A novel triangular solar air collector assisted air source heat pump (TSAHP) is presented, and three working modes of TSAHP are illustrated. The optimal working mode under different operating conditions is determined according to COP. Based on the optimal working mode, the energy, exergy, economy and environment (4E) are compared and analyzed between the TSAHP with three areas of triangular solar air collector (TSAC) and the conventional air source heat pump (ASHP). The main conclusions are drawn as follows:

(1) Increasing TSAC area can effectively reduce energy consumption and improve COP. Power consumption of scenario 3 is 321.9 kWh lower than scenario 4 in the whole heating period.

(2) The exergy efficiency of the TSAHP on parallel working mode is higher than that in series working mode. When the solar irradiance and outdoor temperature are high, the exergy efficiency of TSAHP is higher than that of

conventional ASHP, and TSAHP with 3 m^2 TSAC can reduce the exergy destruction of ASHP components by 784.6 MJ during the whole heating period.

(3) In the 20 beneficial years, the life cycle cost of TSAHP with 3 m^2 TSAC is 18.4% less than that of conventional ASHP, and the TSAHP has more economic advantages at low nominal interest rate and high electric power cost.

(4) The production of TSAC leads to 16 times CO_2 emissions than transportation, and based on the whole life cycle, 1 m^2 of TSAC can reduce CO_2 emission by more than 4500 kg.

Acknowledgement

This work was supported by the National Key R&D Program of China (No. 2020YFD1100304).

Appendix A.

Table A.1 The technical characteristics of the TSAC.

TSAC	Section size: 2.4×2.1×1.2 (m×m×m), width: 0.5/1/1.5 (m)
Glass cover	Materials: Polycarbonate; Size: 2.4×0.7×0.008 (m×m×m) Physical parameter: k_{gc}=0.2 (W/(m·K)); τ_{gc}=0.82; α_{gc}=0.1; ε_{gc}=0.67
Perforated corrugated absorber	Materials: Stainless steel Size: 0.65/0.80/1.39×0.7×0.00015 (m×m×m); Physical parameter: k_{ab}=14.8 (W/(m·K)); α_{ab}=0.92; ε_{ab}=0.2;
Insulation housing	Materials: Polystyrene board and galvanized sheet Physical parameter: k_{ho}=0.028 (W/(m·K)); ε_{ho}=0.1

Table A.2 The technical characteristics of evaporator and condenser.

	Evaporator	Condenser
Size	0.62×0.34×0.03 (m×m×m)	0.86×0.50×0.022 (m×m×m)
Fin	Materials: Aluminum; Area: 7.31 (m^2)	Materials: Aluminum; Area: 12.66 (m^2)
	Thickness: 1.02×10^{-4}; Number: 488;	Thickness: 7.62×10^{-5}; Number: 625;
Tube	Materials: Copper;	Materials: Copper;
	Number: 16 + 16 (two branches)	Number: 12 + 12 (two branches)
	Rows: 2; Length: 19.84 (m);	Rows: 1; Length: 20.57 (m);
	Inside/Outside diameter: 5.2/6.8 (mm)	Inside/Outside diameter: 4.9/6.5 (mm)

Table A.3 The technical characteristics of compressor.

Compressor	
Type	rotary-piston type compressor
Effective displacement	9.16787×10^{-6} (m^3)
Clearance volume fraction	3.17178×10^{-2}
Loss in effective displacement per unit back pressure	2.42768×10^{-5} (m^3/kPa)

Table A.4 The parameter of refrigerant.

R410a	50% R32+50% R125
Boiling point	-51.6 ℃
Freezing point	-155 ℃
Critical temperature	72.5 ℃
Critical pressure	4.95 Mpa
Ozone destruction potential (ODP)	0.000
Global warming coefficient (GWC)	1730
Critical density	0.500 g/cm^3

Table A.5 Geometric and physical parameters of the rural residence.

Rural residence	Size: 3×6×6 (m×m×m)
Window	Heat transfer coefficient: 0.35 (W/(m^2·K))
	Window-wall ratio: 0.3
	Position: The south wall of rural residence
Door	Heat transfer coefficient: 2.8 (W/(m^2·K))
	Size: 2.3×1 (m×m)
	Position: The south wall of rural residence

Heat transfer coefficient: 2.5 (W/(m^2·K))

Appendix B.

The heat transfer element of TSAC is calculated as follows:

$$Q_{\text{sol.gc}}=a_{\text{gc}}A_{\text{gc}}I_{\text{gc}} \tag{B.1}$$

$$Q_{\text{conv.gc-outdoor}}=h_{\text{conv.gc-outdoor}}A_{\text{gc}}\left(T_{\text{outdoor}}-T_{\text{gc}}\right) \tag{B.2}$$

$$Q_{\text{conv.gc-air}}=h_{\text{conv.gc-air}}A_{\text{gc}}\left(T_{\text{air}}-T_{\text{gc}}\right) \tag{B.3}$$

$$Q_{\text{rad.gc-outdoor}}=h_{\text{rad.gc-outdoor}}A_{\text{gc}}\left(\sqrt[4]{\frac{1+\cos\beta_{\text{gc}}}{2}}\varepsilon_{\text{sky}}+\frac{1-\cos\beta_{\text{gc}}}{2}T_{\text{outdoor}}-T_{\text{gc}}\right) \tag{B.4}$$

$$Q_{\text{sol.ab}}=a_{\text{ab}}A_{\text{ab}}I_{\text{ab}} \tag{B.5}$$

$$Q_{\text{conv.ab-air}}=h_{\text{conv.ab-air}}A_{\text{ab}}\left(1-P_{\text{h}}\right)\left(T_{\text{air}}-T_{\text{ab}}\right) \tag{B.6}$$

$$Q_{\text{conv.hole}}=h_{\text{conv.hole}}A_{\text{ab}}\frac{4d_{\text{ab}}P_{\text{h}}}{D}\left(T_{\text{ab}}-T_{\text{air}}\right) \tag{B.7}$$

$$Q_{\text{conv.ho-air}}=h_{\text{conv.ho-air}}A_{\text{ho}}\left(T_{\text{ho}}-T_{\text{air}}\right) \tag{B.8}$$

$$Q_{\text{u.air}}=m_{\text{air}}c_{\text{p.air}}\left(T_{\text{air.out}}-T_{\text{air.in}}\right) \tag{B.9}$$

The heat transfer coefficients $h_{\text{conv.gc-od}}$ and $h_{\text{rad.gc-od}}$ were proposed by Watmuff et al. (1977), and Kumar et al. (2009), the $h_{\text{conv.gc-air}}$, $h_{\text{conv.ab-air}}$ and $h_{\text{conv.ho-air}}$ were proposed by Leon and Kumar (2007), and the $h_{\text{conv.hole}}$ was proposed by Vandecker et al. (2001).

Appendix C.

The heat exchange efficiency ε_{r} of single-phase region which includes de-superheating, subcooling and superheating region was presented by McQuiston and Parker (1982).

$$\varepsilon_{\text{r}}=1-\exp\left(NTU^{0.22}\left(\exp\left(-\frac{C_{\min}}{C_{\max}}NTU^{0.78}\right)-1\right)\right) \tag{C.1}$$

$$NTU = \frac{UA}{C_{\min}} \tag{C.2}$$

$$C_{\min} = ym_{air} \min(c_{\text{p.air}}; \left| \frac{i_{\text{out}} - i_{\text{in}}}{T_{\text{ref.out}} - T_{\text{ref.in}}} \right|) \tag{C.3}$$

$$C_{\max} = ym_{air} \max(c_{\text{p.air}}; \left| \frac{i_{\text{out}} - i_{\text{in}}}{T_{\text{ref.out}} - T_{\text{ref.in}}} \right|) \tag{C.4}$$

The heat exchange efficiency of condensing and evaporating region was as follows (Mcquiston et al.,1982):

$$\varepsilon_{\text{r}} = 1 - \exp\left(\frac{-UA}{C} \right) \tag{C.5}$$

$$C = ym_{air} c_{\text{p.air}} \tag{C.6}$$

The evaporator and condenser in this study were finned-tube exchangers, and the total thermal resistance was derived as follows:

$$\frac{1}{UA} = \frac{1}{\eta_{\text{tf}} h_{\text{out}} A_{\text{out}}} + \frac{\ln\left(d_{\text{out}}/d_{\text{in}}\right)}{2\pi Lk} + \frac{1}{h_{\text{in}} A_{\text{in}}} \tag{C.7}$$

The total finned efficiency η_{tf} was proposed by McQuiston and Parker (1982), the convective heat transfer coefficient on the outside surface of the finned-tube exchanger h_{out} was presented by Gary and Webb (1986), and the convective heat transfer coefficient of the inside surface h_{in} was proposed by T. Zakula et al. (2011).

References

Armstrong P. R. Jiang W., Winiarski D., Katipamula S., Norford L. K. Willingham, R. A., 2014. Efficient Low-Lift Cooling with Radiant Distribution, Thermal Storage, and Variable-Speed Chiller Controls—Part I: Component and Subsystem Models. HVAC&R Research 25, 09-54.

http://dx.doi.org/10.1080/10789669.2009.10390842

Afshari F., Comakli O., Adiguzel N., Zavaragh H. G., 2017. Influence of refrigerant

properties and charge amount on performance of reciprocating compressor in air source heat pump. Journal of Energy Engineering 143, 04016025.

doi:10.1061/(ASCE)EY.1943-7897.0000377

Afshari F., Karagoz S., Comakli O., Zavaragh H. G., 2019. Thermodynamic analysis of a system converted from heat pump to refrigeration device, Heat and Mass Transfer, 55, 281–291.

doi:10.1007/s00231-018-2412-5

Cai J., Ji J., Wang Y., Huang W., 2017. Operation characteristics of a novel dual source multi-functional heat pump system under various working modes. Applied Energy 194, 236-246.

http://dx.doi.org/10.1016/j.apenergy.2016.10.075

Chen H., Wang Y., Li J., Cai B., Zhang F., Lu T., Yang J., Jiang L., Zhang Y., Zhou J.,2020. Experimental research on a solar air-source heat pump system with phase change energy storage. Energy & Buildings 228, 110451.

https://doi.org/10.1016/j.enbuild.2020.110451

Chen Y., Yang J., Berardi U., Cui G., Li R., Li N., 2022. Assessments of multiple operation strategies in a passive office Building in Cold Region of China. Energy & Buildings 254, 111561.

https://doi.org/10.1016/j.enbuild.2021.111561

Deniz E., Cinar S., 2016. Energy, exergy, economic and environmental (4E) analysis of a solar desalination system with humidification-dehumidification. Energy Conversion

and Management 126, 12-19.

http://dx.doi.org/10.1016/j.enconman.2016.07.064

Esen M., 2000. Thermal performance of a solar-aided latent heat store used for space heating by heat pump. Solar Energy 69, 15-25.

doi:10.1016/S0038-092X(00)00015-3

Esen H., Inalli M., Esen M., Pihtili K., 2007. Energy and exergy analysis of a ground-coupled heat pump system with two horizontal ground heat exchangers. Building and Environment 42, 3606-3615.

doi:10.1016/j.buildenv.2006.10.014

Gray D. L., Webb R. L., 1986. Heat transfer and friction correlation for plate finned-tube heat exchangers having plain fins. Proceedings of 8th International Heat Transfer Conference 6, 2745–2750.

Hassan H., Yousef M. S., Abo-Elfadl S., 2021. Energy, exergy, economic and environmental assessment of double pass V-corrugated-perforated fnned solar air heater at different air mass ratios. Sustainable Energy Technologies and Assessments. Sustainable Energy Technologies and Assessments 43, 100936.

https://doi.org/10.1016/j.seta.2020.100936

Jiang Y., Zhang H., Wang Y., You S., Wu Z., Fan M., Wang L., Wei S., 2021. A comparative study on the performance of a novel triangular solar air collector with tilted transparent cover plate. Solar Energy 227, 224-235.

https://doi.org/10.1016/j.solener.2021.08.083

Jiang Y., Zhang H., Zhao R., Wang Y., Liu M., You, S., Wu Z., Liu Z., Wei S., 2022. Research on the operation strategies of the solar assisted heat pump with triangular solar air collector. Energ 246, 123398.

doi:10.1016/j.energy.2022.123398

Kumar A., Bhagoria J. L., Sarviya R. M., 2009. Heat transfer and friction correlations for artificially roughened solar air heater duct with discrete W-shaped ribs. Energy Conversion and Management 50, 2106-2117.

doi:10.1016/j.enconman.2009.01.025

Kegel M., Tamasauskas J., Sunye R., Langlois A., 2012. Assessment of a solar assisted air source and a solar assisted water source heat pump system in a Canadian household. Energy Procedia 30, 654-663.

doi: 10.1016/j.egypro.2012.11.074

Kavian S., Aghanajafi C., Mosleh H. J., Nazari A., Nazari A., 2020. Exergy, economic and environmental evaluation of an optimized hybrid photovoltaic-geothermal heat pump system. Applied Energy 276, 115469.

http://dx.doi.org/10.1016/j.enconman.2016.07.064

Leon M. A., Kumar S., 2007. Mathematical modeling and thermal performance analysis of unglazed transpired solar collectors. Solar energy 81, 62-75.

doi:10.1016/j.solener.2006.06.017

Long J., Zhang R., Lu J., Xu F., 2019. Heat transfer performance of an integrated solar-air source heat pump evaporator. Energy Conversion and Management 184, 626-635.

https://doi.org/10.1016/j.enconman.2019.01.094

Long T., Qiao Z., Wang M., Li Y., Lu J., Li W., Zeng L., Huang S., 2020. Performance analysis and optimization of a solar-air source heat pump heating system in Tibet, China. Energy & Buildings 220, 110084.

https://doi.org/10.1016/j.enbuild.2020.110084

Liu Z., Liu Y., Wu D., Jin G., Yu H., Ma W., 2020. Performance and feasibility study of solar-air source pump systems for low-energy residential buildings in Alpine regions. Journal of Cleaner Production 256, 120735.

https://doi.org/10.1016/j.jclepro.2020.120735

Mcquiston F. C., Parker J. D., Spitler J. D., 1982. Heating, ventilating, and air conditioning: analysis and design. John Wiley & Sons, Inc.

Petela R., 2003. Exergy of undiluted thermal radiation. Solar Energy 74, 469-448.

doi:10.1016/S0038-092X(03)00226-3

Pater S., 2019. Field measurements and energy performance analysis of renewable energy source devices in a heating and cooling system in a residential building in southern Poland. Energy and Buildings 199, 115-125.

doi:10.1016/j.enbuild.2019.06.057

Rout A., Singh S., Mohapatra T. Sahoo S. S., Solanki C. S., 2021. Energy, exergy, and economic analysis of an off-grid solar polygeneration system. Energy Conversion and Management 238, 114177.

https://doi.org/10.1016/j.enconman.2021.114177

Saloux E., Sorin M., Teyssedou A.,2019. Exergo-economic analyses of two building integrated energy systems using an exergy diagram. Solar Energy 189, 333-343.

https://doi.org/10.1016/j.solener.2019.07.070

Safijahanshahi E., Salmanzadeh M., 2019. Performance simulation of combined heat pump with unglazed transpired solar collector. Solar Energy 180, 575-593.

https://doi.org/10.1016/j.solener.2019.01.038

Singh A., Sarkar J., Sahoo R. R., 2020a. Experimentation on solar-assisted heat pump dryer: Thermodynamic, economic and exergoeconomic assessments. Solar Energy 208, 150-159.

https://doi.org/10.1016/j.solener.2020.07.081

Singh A., Sarkar J., Sahoo R. R., 2020b. Experimental energy, exergy, economic and exergoeconomic analyses of batch-type solar-assisted heat pump dryer. Renewable Energy 156, 1107-1116.

https://doi.org/10.1016/j.renene.2020.04.100

Song Z., Ji J., Li Z., Wang, 2021a. Comparison analyses of three photovoltaic solar-assisted heat pumps based on different concentrators. Energy & Buildings 251, 111348.

https://doi.org/10.1016/j.enbuild.2021.111348

Song Z., Ji J., Cai J., Zhao B., Li Z., 2021b. Investigation on a direct-expansion solar-assisted heat pump with a novel hybrid compound parabolic concentrator/photovoltaic/fin evaporator. Applied Energy 299, 117279.

https://doi.org/10.1016/j.apenergy.2021.117279

Sakellariou E. I., Axaopoulos P. J., Wright A. J., 2021. Energy and economic evaluation of a solar assisted ground source heat pump system for a north Mediterranean city. Energy & Buildings 231, 110640.

https://doi.org/10.1016/j.enbuild.2020.110640

Treichel C., Cruickshank C. A., 2021a. Economic analysis of heat pump water heaters coupled with air-based solar thermal collectors in Canada and the United States. Journal of Building Engineering 35, 102034.

https://doi.org/10.1016/j.jobe.2020.102034

Treichel C., Cruickshank C. A., 2021b. Greenhouse gas emissions analysis of heat pump water heaters coupled with air-based solar thermal collectors in Canada and the United States. Energy & Buildings 231, 110594.

https://doi.org/10.1016/j.enbuild.2020.110594

Treichel C., Cruickshank C. A., 2021c. Energy analysis of heat pump water heaters coupled with air-based solar thermal collectors in Canada and the United States. Energy 221, 119801.

https://doi.org/10.1016/j.energy.2021.119801

Ural T., Kecebas A., Guler O. V., 2021a. Thermodynamic performance evaluation of a heat pump system with textile based solar air heater for heating process. Applied Thermal Engineering 191, 116905.

https://doi.org/10.1016/j.applthermaleng.2021.116905

Ural T., Dolgun G. K., Guler O. V., Kecebas A., 2021b. Performance analysis of a textile

based solar assisted air source heat pump with the energy and exergy methodology. Sustainable Energy Technologies and Assessments 47, 101534.

https://doi.org/10.1016/j.seta.2021.101534

Vandecker G. W. E., Hollands K. G. T., Brunger A. P., 2001. Heat-exchange relations for unglazed transpired solar collectors with circular holes on a square or triangular pitch. Solar Energy 71, 33-45.

Doi:10.1016/s0038-092x(01)00014-7

Watmuff J. H., Charters W. W. S., Proctor D., 1977. Solar and wind induced external coefficients - solar collectors. COMPLES, 2-56.

Zakula T., Gayeski N. T., Armstrong P. R., Norford L. K., 2011. Variable-speed heat pump model for a wide range of cooling conditions and loads. HVAC&R Research, 670-691.

http://dx.doi.org/10.1080/10789669.2011.607745